

Wave-induced seabed response around an offshore pile foundation platform



Qi Zhang^{a,b}, Xiang-Lian Zhou^{a,b,*}, Jian-Hua Wang^c, Jun-Jie Guo^{a,b}

^a Collaborative Innovation Center for Advanced Ship and Deep-Sea Exploration (CISSE), Shanghai 200240, PR China

^b State Key Laboratory of Ocean Engineering, Shanghai Jiao Tong University, Shanghai 200240, PR China

^c Centre for Marine Geotechnical Engineering, Shanghai Jiao Tong University, Shanghai 200240, PR China

ARTICLE INFO

Keywords:

Pile foundation platform
Porous seabed
Wave motion
 u - p Model

ABSTRACT

In this paper, a three-dimensional integrated numerical model including the wave and seabed sub-model is developed to investigate the wave induced seabed response around a pile foundation platform. The wave sub-model is based on Volume-Averaged Reynolds-Averaged Navier-Stokes (VARANS) equations with k - ϵ turbulence closure scheme, and the volume of fluid (VOF) method is applied to track water free surface. The seabed is treated as an isotropic and homogeneous porous medium and characterized by Biot's partly dynamic equations (u - p model). The proposed model is verified with the previous analytical results. Based on the numerical results, the distribution of flow field around pile foundation will be investigated. Then, a comprehensive comparison between a pile foundation platform model and a pile foundation without platform model will be performed to examine the effects of platform to the pile foundation. Finally, the effects of wave, pile foundation, and seabed characteristics, such as wave depth, wave height, pile diameter, pile insertion ratio, soil permeability and degree of saturation on the wave-induced seabed and pile foundation platform response will be studied.

1. Introduction

In recent years, offshore platform have been widely used in mining oil and nature gas under the seabed in marine engineering. Offshore pile foundations are one of the most commonly used foundation concepts in offshore platform, especially in areas with relatively shallow water. Wave force is one of the major forces the offshore pile foundation endures, and the effect of wave load on the offshore pile foundation reflected in two aspects: one is the dynamic response of seabed around pile foundation under wave loading. The dynamic wave pressure acting on the seabed surface will induce excess pore pressure, which is directly related to the stability and safety of the seabed. With pore pressure increasing and vertical effective stress decreasing, the seabed may become unstable or even liquefied. The other is that pile foundation under wave loading may lead to large displacement and complicated bending moment along the vertical direction of the pile foundation, which will closely lead to the instability of pile foundation platform, or even collapse. Therefore, it is essential to make a proper evaluation on the dynamic response of seabed around pile foundation platform such as the pore pressure of seabed, displacement and bending moment of pile foundation, which can judge the stability and safety of the pile foundation.

Many theories had been developed for the wave-induced seabed

response based on different assumptions of the rigidity of soil skeleton and the compressibility of pore fluid. Among these, researchers treated the seabed as a single phase medium (Gade, 1958; Hsiao and Shemdin, 1980; Mei and Liu, 1987) or a rigid porous medium (Sleath, 1970; Liu, 1973), in which the pore pressure of seabed could not be reflected in a single medium. Sleath (1970) proposed an analytical solution to compare with laboratory experiments on wave-induced soil response in two different beds of sand, which assumed that the seabed was rigid and permeable and the pore fluid was incompressible and followed Darcy's law. Based on this, Moshagen and Torum (1975) proposed an analytical solution for the wave-induced seabed response with assumptions of a rigid and permeable sandy seabed but the pore fluid was compressible. Biot (1956, 1962) proposed the consolidation theory, which can be used to investigate the wave-induced seabed response, with the assumptions that the porous medium was deformable and compressible. Based on Biot's theory, there have three kinds of formulations in analysis the wave-induced seabed response: Quasi-static (QS), Partly-dynamic (u - p) and Fully-dynamic (u - w). Quasi-static (QS) condition had considered to analysis the response of seabed under wave loading (Yamamoto, 1977, 1981; Yamamoto et al., 1978; Madsen, 1978; Seymour, 1996; Lin et al., 1997; Jeng et al., 1997), where the acceleration of soil skeleton and porous fluid had not been considered. Zienkiewicz et al., (1980) proposed the u - p approximation

* Corresponding author at: State Key Laboratory of Ocean Engineering, Shanghai Jiao Tong University, Shanghai 200240, PR China.
E-mail addresses: zhouxi99@hotmail.com, zhouxi@sjtu.edu.cn (X.-L. Zhou).

to porous flow through one-dimensional analysis, and the respective ranges of validity of the QS and $u-p$ formulations had also been examined in investigating the wave-induced soil response. Based on the continuum theory, Mei and Foda (1981) proposed a boundary-layer approximation to investigate the wave-induced soil response, in which both the coarse and fine sand were concerned. Hsu and Jeng (1994) proposed a closed-form analytical solution to study the wave-induced soil response in a finite thickness seabed of fine sand, where the boundary-layer approximation was proved to be limited. Yuhi and Ishida (1998) proposed an analytical solution to solve the boundary value problem directly instead of using the boundary layer approximation. Based on the $u-p$ approximation, Jeng et al (1999) proposed an analytical solution of dynamic response for a porous seabed under wave loading through two-dimensional analysis, and the relative difference between the governing equations with inertia forces and without inertia forces had been discussed. Jeng and Cha (2003) further investigated the dynamic response of a finite thickness seabed under wave loading based on the $u-p$ approximation and $u-w$ approximation, in which the dynamic soil behavior and wave nonlinearity were examined. Ulker et al. (2009) developed a set of generalized analytical solutions for the dynamic response of a saturated porous seabed under wave loading, and the applicability of the three formulations were identified. Zhou et al. (2011) applied the Fourier transformation and Transmission and reflection Matrix method to investigate wave-induced seabed response in a multi-layered poro-elastic seabed. Then, Zhou et al. (2014) investigated the dynamic response of a porous seabed under cnoidal wave based on the $u-p$ approximation and the liquefaction phenomenon of seabed under wave loading in shallower water region had been studied.

Similarly, many investigations had been developed to understand the mechanisms of wave and offshore piles interaction. The effects of various wave characteristics on offshore piles have been investigated and discussed by many researchers in the early years (Chakarabarti and Tam, 1975; Raman et al., 1977; Au and Brebbia, 1983). Mitwally and Novak (1987) investigated the dynamic interaction between piles under wave loading and the pile group properties of an offshore tower which included the main characteristics such as the natural frequencies, mode shapes and damping. Bushnell (1977) conducted a series of experiment focus on the flow interference effects between two piles and a 3×3 array subjected to harmonic oscillating flow. Eicher et al. (2003) developed a numerical model to investigate the effects of an offshore concrete pile under combined loading conditions and the effects of varying the loading parameters. Lu and Jeng (2008) proposed a coupled numerical model, which included the seawater, seabed and pile, to investigate the dynamic response of a porous seabed and offshore pile to wave loadings. Zhang and Li (2011) developed a numerical model to analyze the internal forces and deformations of an offshore monopile by the dynamic $p-y$ method under wave loading, where p refers to the lateral soil pressure per unit length of pile and y refers to the lateral deflection. Li et al. (2011) proposed a three-dimensional numerical model to investigate wave-induced transient and residual pore pressure responses around a pile foundation. Cuéllar et al. (2012) investigated the possible influence of transient changes of pore water pressure around a pile foundation by theoretic methods and means of model tests in a reduced scale, respectively, and some main factors were discussed which was closely related to the generation of pore pressure around the pile foundation. Sui et al. (2013) developed a three-dimensional integrated model to study wave-induced seabed response and liquefaction potential around pile foundation, in which Boussinesq wave mode was used to simulate the wave-pile interaction and Biot's poro-elastic theory is solved for the seabed deformation, effective stresses and pore pressure in soil. Zhang et al. (2015) established a dynamic finite element model to examine the dynamic response of an all-vertical-piled wharf under wave cyclic loads and proposed a simplified dynamic numerical method based on the $p-y$ curve.

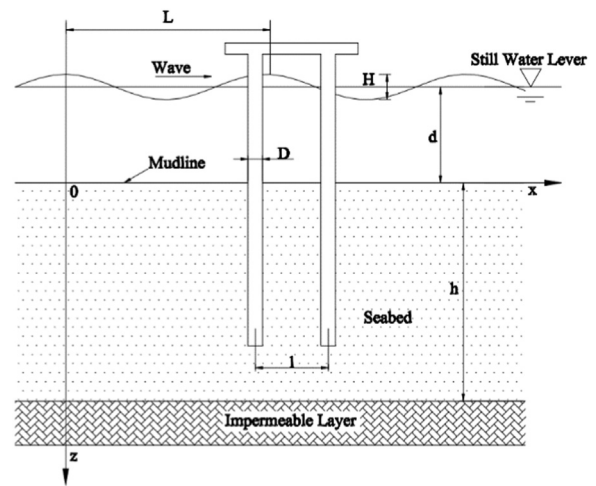
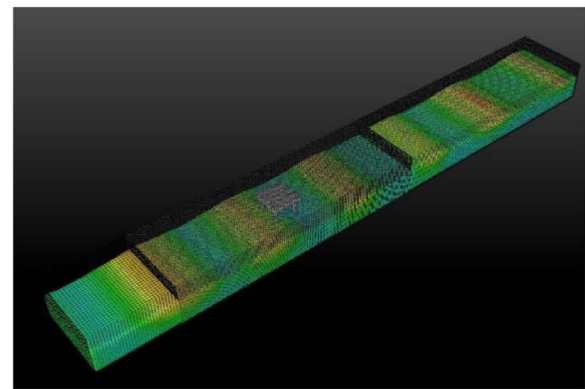
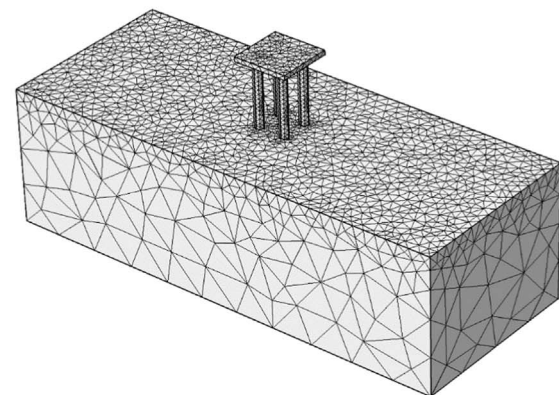


Fig. 1. The calculation model.



a. wave sub-model



b. seabed sub-model

Fig. 2. The mesh of the (a) wave sub-model and (b) seabed sub-model.

The methods of investigating the fluid-structure-seabed interaction (FSSI) problem (including fluid-seabed interaction problem) could be divided into three kinds: the uncoupled method, one-way coupled method (also called semi-coupled method) and fully coupled method. In the uncoupled model, the fluid part and the seabed part were studied separately and there was no data exchange between the fluid domain and seabed domain. A simplified wave pressure equation was often adopted to simulate the wave propagation over the seabed (Hsu and Jeng, 1994; Ulker et al., 2009; Zhou et al., 2011). The one-way coupled model, which also called the semi-coupled model in some previous investigations, was adopted widely in analyzing the wave-seabed-

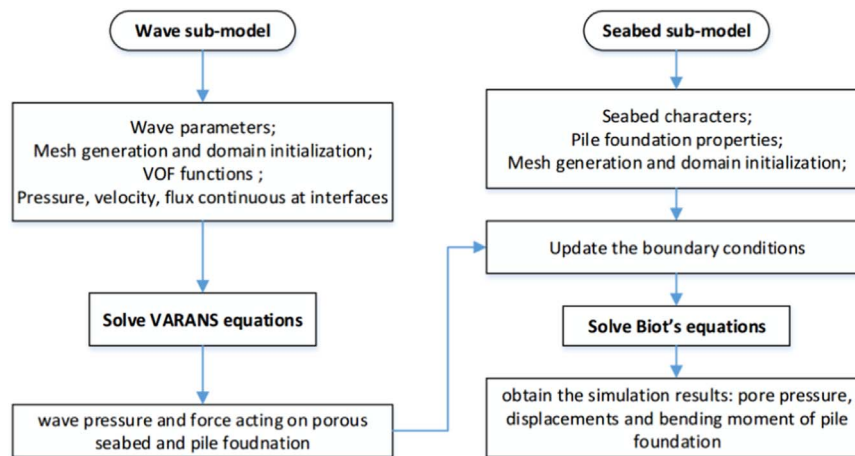


Fig. 3. The working procedure of the integrated model.

Table 1
Input data for comparison.

Wave characteristics			
Wave height (H)	2 (m)	Water depth (d)	70 (m)
Wave period (T)	15 (s)	Wave length (L)	311.59 (m)
Water Characteristics			
Density (ρ_w)	1000 (kg/m ³)	Modulus of volume (k_w)	2×10^9 (N/m ²)
Seabed Characteristics			
Seabed thickness (h)	25 (m)	Density (ρ_s)	1850 (kg/m ³)
Seabed length (l)	700 (m)	Shear modulus (G)	1×10^7 (N/m ²)
Passion ratio (ν)	0.333	Permeability (k_z)	1×10^{-2} (m/s)
Porosity (n)	0.3	Degree of saturation (S_r)	1

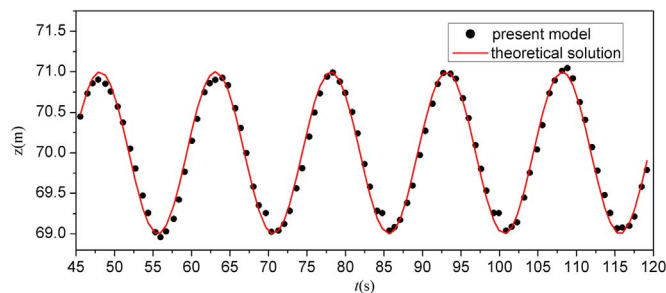


Fig. 4. Comparisons of computed water surface elevations with the theoretical solution and the present model.

structure problems (Chen and Hsu, 2005; Jeng et al., 2013). This method mainly considered the effects of one domain to another domain (like the effects of seabed parameters induce wave damping and the wave-induced seabed response), which need to be noticed is that there is no feedback from the second domain to the first domain (Ye et al., 2013, 2016). The fully coupled method was also studied in some previous researches (Mostafa et al., 1999; Karunarathna and Lin, 2006). To the fully coupled method, more than two physical domains need to be calculated simultaneously and a real-time data exchange is required between the different domains (like the fluid domain and the seabed domain), which requires a significant amount of computing resources and it is hard to calculate some complex 3-D FSSI problems. As to this research, our main purpose is to investigate the wave-induced seabed response. Therefore, a one-way coupled model (the semi-coupled model) was developed to study the seabed response under wave loading with a data transmission from the wave sub-model to the seabed sub-model. This is reasonable when the deformations of

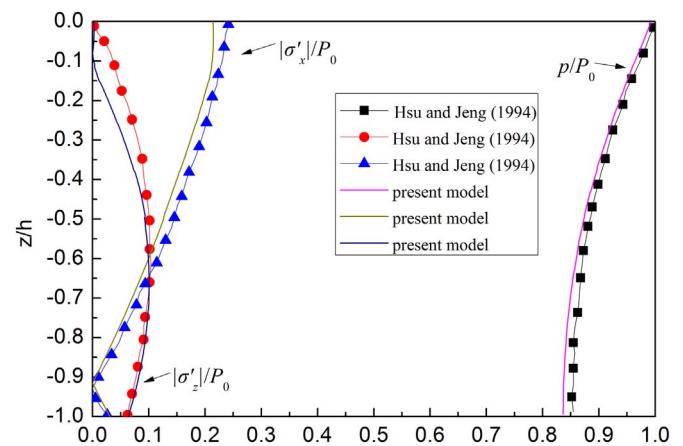


Fig. 5. Comparison of the linear wave-induced seabed response between the present model and the previous analytical solution (Hsu and Jeng, 1994).

the seabed are small and the wave-induced seabed response generally is apparently minor comparing with the wave length from the point view of physics (Jeng, 2001; Liu et al., 2007).

To date, the wave-induced seabed response around a pile foundation had not been fully understood because of the complicated behavior and interaction among wave, seabed and pile foundation. Most of the investigations focused on the wave-induced seabed and monopile foundation response. However, the behavior of a pile group foundation under wave loading is more complicated because of the interaction between piles and the existence of the phase difference between piles. Moreover, only a few researchers had concerned the effect of the existence of the platform on the behavior of pile foundation under wave loading. The existence of a platform will change the mechanical behavior of the pile foundation and seabed significantly. Therefore, it is necessary to understand the behavior of an appropriate model for the wave-seabed-pile foundation platform system.

The main objective of this paper is to investigate the wave-induced seabed and platform response. A three-dimensional FEM model including the wave, seabed and a typical 2×2 pile foundation platform is adopted for the investigation. A Volume-Averaged Reynolds-Averaged Navier-Stokes (VARANS) solver with volume of fluid (VOF) method and $k-\epsilon$ turbulence model is developed for modeling wave propagation. The Biot's partly dynamic equation ($u-p$ model), which both displacement and pore pressure are the field variables, is adopted considering the acceleration of soil skeleton. The present model is verified with the previous analytical results and shows good agreement. Then, the distribution of flow field influenced by the pile foundation is investigated. Moreover, a comprehensive comparison between a pile

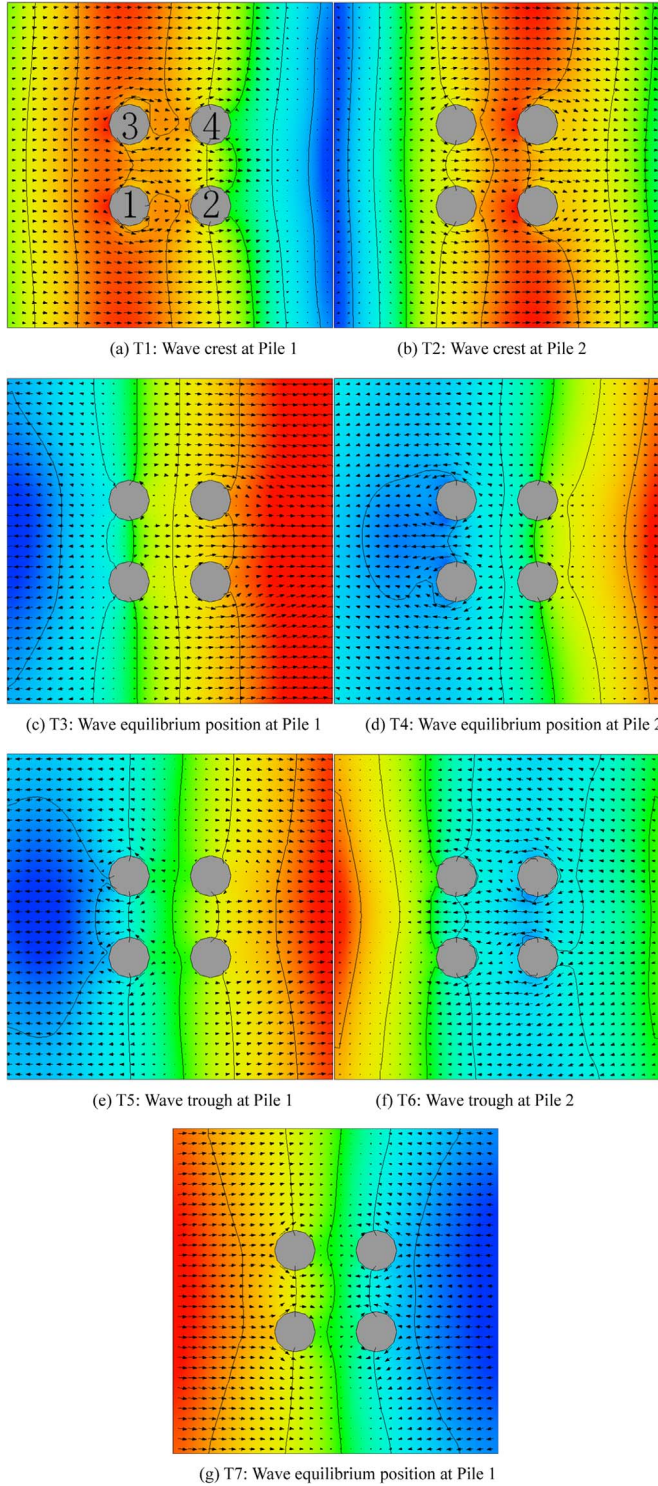


Fig. 6. The distribution of wave velocity vector and wave pressure around the array of piles at the depth $z=0.35$ m in one wave period.

foundation and a pile foundation platform is performed to examine the effects of platform to the pile foundation. Finally, the effects of wave parameters (wave depth and wave height), pile foundation properties (pile diameter and pile insertion ratio) and seabed characteristics (soil permeability and degree of saturation) on the wave motion and seabed response around the pile foundation platform will be studied.

Table 2
Input data of standard case.

Wave Characteristics			
Wave height (H)	1.5 (m)	Water depth (d)	10 (m)
Wave period (T)	8 (s)	Wave length (L)	71.7 (m)
Water Characteristics			
Density (ρ_w)	1000 (kg/m ³)	Modulus of volume (k_w)	2×10^9 (N/m ²)
Seabed Characteristics			
Seabed thickness (h)	30 (m)	Density (ρ_s)	1850 (kg/m ³)
Seabed length (l)	100 (m)	Shear modulus (G)	1.12×10^{10} (N/m ²)
Passion ratio (ν)	0.25	Permeability (k_z)	1×10^{-2} (m/s)
Porosity (n)	0.4	Degree of saturation (S_r)	0.98
Pile Characteristics			
Young's modulus (E_p)	2.8×10^{10} (N/m ²)	Density (ρ_p)	2300 (kg/m ³)
Passion ratio (ν_p)	0.25	Pile diameter (D)	2 (m)
Pile length (d_p)	35 (m)	Insertion ratio (K_p)	0.4
Pile spacing (l_p)	6 (m)		

2. Governing equations

In this study, we consider the wave-induced pore pressure of the porous seabed and the response of the pile foundation platform. As shown in Fig. 1, the calculation model can be divided into two sub models: the wave sub-model and seabed sub-model.

2.1. Governing equations of flow

The VARANS equation, mass conservation and momentum conservation equations are adopted as the governing equation for the incompressible fluid motion (Masuoka and Takatsu, 1996; Nakayama and Kuwahara, 1999; Hsu et al., 2002).

$$\frac{\partial \langle u_{fi} \rangle}{\partial x_i} = 0 \quad (1)$$

$$\begin{aligned} \frac{\partial \rho_f \langle u_{fi} \rangle}{\partial t} + \frac{\partial \rho_f \langle u_{fi} \rangle \langle u_{fj} \rangle}{\partial x_j} = & -\frac{\partial \langle p_f \rangle}{\partial x_i} + \frac{\partial}{\partial x_j} \left[\mu \left(\frac{\partial \langle u_{fi} \rangle}{\partial x_j} + \frac{\partial \langle u_{fj} \rangle}{\partial x_i} \right) \right] \\ & + \frac{\partial}{\partial x_j} (-\rho_f \langle u'_i u'_j \rangle) + \rho_f g_i \end{aligned} \quad (2)$$

where x_i is the Cartesian coordinate, ρ_f is the density of fluid, $\langle u_{fi} \rangle$ is the ensemble mean velocity; μ is dynamic viscosity, $\langle p_f \rangle$ is fluid pressure, t is time, and g_i is the gravitation acceleration. The Reynolds stress term, $-\rho_f \langle u'_i u'_j \rangle$, is modeled by the 2-equations k - ϵ turbulence model (Lauder and Spalding, 1974; Rodi, 1993). By applying eddy-viscosity assumption, the Reynolds stress term can be estimated by

$$-\rho_f \langle u'_i u'_j \rangle = \mu_t \left[\frac{\partial \langle u_{fi} \rangle}{\partial x_j} + \frac{\partial \langle u_{fj} \rangle}{\partial x_i} \right] - \frac{2}{3} \rho_f \delta_{ij} k \quad (3)$$

where μ_t is the turbulent viscosity, k is the turbulence kinetic energy (TKE), and δ_{ij} is the Kronecker delta. Substituting Eq. (3) into Eq. (2), the Eq. (2) can be rewritten as

$$\begin{aligned} \frac{\partial \rho_f \langle u_{fi} \rangle}{\partial t} + \frac{\partial \rho_f \langle u_{fi} \rangle \langle u_{fj} \rangle}{\partial x_j} = & -\frac{\partial}{\partial x_i} \left[\langle p_f \rangle + \frac{2}{3} \rho_f k \right] \\ & + \frac{\partial}{\partial x_j} \left[\mu_{eff} \left(\frac{\partial \langle u_{fi} \rangle}{\partial x_j} + \frac{\partial \langle u_{fj} \rangle}{\partial x_i} \right) \right] + \rho_f g_i \end{aligned} \quad (4)$$

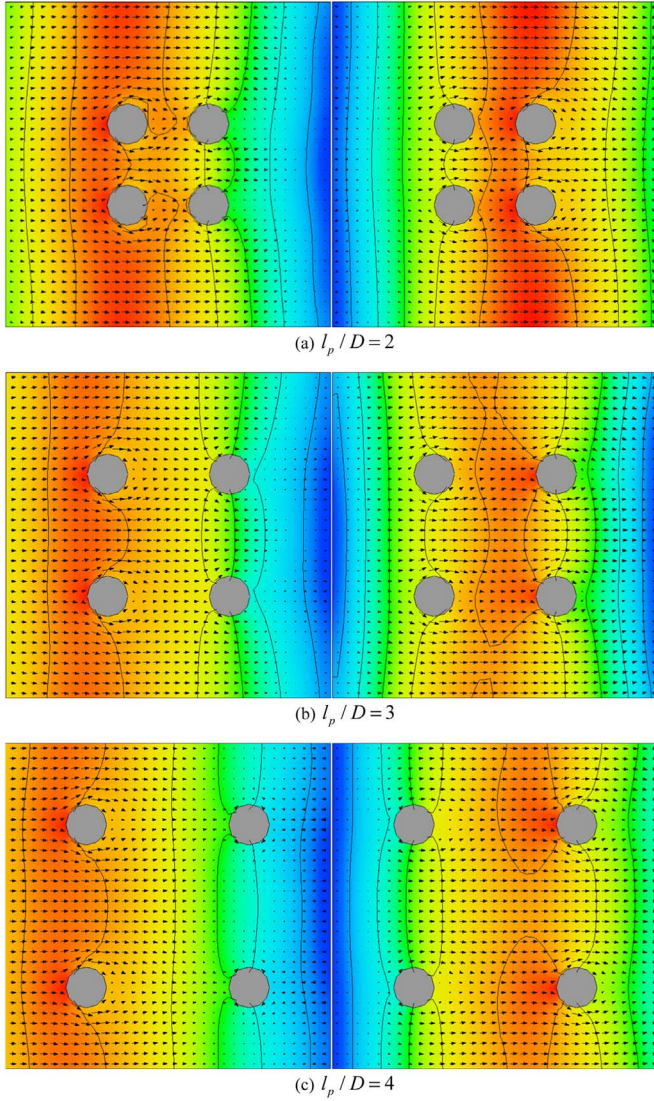


Fig. 7. The vector field and the distribution of wave pressure around the 2×2 array of piles at the depth $z=0.35$ m when the wave crest reaches to Pile 1 and Pile 2 for various non-dimensional pile spacing.

in which $\mu_{eff} = \mu + \mu_t$ is the total effective viscosity.

A sophisticated and widely used equation for k - ϵ turbulence model which consists of two transport equations for the turbulent kinetic energy and its dissipation can be expressed as (Launder and Spalding, 1974)

$$\frac{\partial \rho k}{\partial t} + \frac{\partial \rho \langle u_j \rangle k}{\partial x_j} = \frac{\partial}{\partial x_j} \left[\left(\mu + \frac{\mu_t}{\sigma_k} \right) \frac{\partial k}{\partial x_j} \right] + \rho P_k - \rho \epsilon \quad (5)$$

$$\frac{\partial \rho \epsilon}{\partial t} + \frac{\partial \rho \langle u_j \rangle \epsilon}{\partial x_j} = \frac{\partial}{\partial x_j} \left[\left(\mu + \frac{\mu_t}{\sigma_\epsilon} \right) \frac{\partial \epsilon}{\partial x_j} \right] + \frac{\epsilon}{k} (C_{\epsilon 1} \rho P_k - C_{\epsilon 2} \rho \epsilon) \quad (6)$$

$$\mu_t = \rho C_\mu \frac{k^2}{\epsilon} \quad (7)$$

in which ϵ is the rate of turbulent energy dissipation, and μ_t is the turbulent kinematic viscosity.

2.2. Governing equations of porous seabed

In this section, Biot's partly dynamic theory, the “ u - p ” approximation, is adopted as the governing equations for the investigation of wave-induced pore pressure of the porous seabed, in which the inertial

forces was not concerned, but including the accelerations of soil particles. Herein, we propose the following assumptions that the seabed is treated as an isotropic and homogeneous porous medium with the same permeability k_z in all directions, the fluid follows Darcy's law, and the water is compressible due to a small degree of unsaturation. These assumptions are reasonable due to the porous seabed is deformable and compressible, together with a high degree of saturation, and the oscillations of wave-induced seabed response are quite small relative to the equilibrium state.

Based on conservation of mass and force balances (Zienkiewicz et al., 1980), the governing equations can be written as

$$k \nabla^2 p - \gamma_w n \beta \frac{\partial p}{\partial t} + k_s \rho_f \frac{\partial^2 \epsilon_s}{\partial t^2} = \gamma_w \frac{\partial \epsilon_s}{\partial t} \quad (8)$$

$$\frac{\partial \sigma'_x}{\partial x} + \frac{\partial \tau_{xy}}{\partial y} + \frac{\partial \tau_{xz}}{\partial z} = \frac{\partial p}{\partial x} + \rho \frac{\partial^2 u}{\partial t^2} \quad (9)$$

$$\frac{\partial \tau_{xy}}{\partial x} + \frac{\partial \sigma'_y}{\partial y} + \frac{\partial \tau_{yz}}{\partial z} = \frac{\partial p}{\partial y} + \rho \frac{\partial^2 v}{\partial t^2} \quad (10)$$

$$\frac{\partial \tau_{xz}}{\partial x} + \frac{\partial \tau_{yz}}{\partial y} + \frac{\partial \sigma'_z}{\partial z} = \frac{\partial p}{\partial z} + \rho \frac{\partial^2 w}{\partial t^2} \quad (11)$$

where k_s is the Darcy's permeability, p is the wave-induced pore pressure, γ_w is the unit weight of water, n is the soil porosity, ρ_f is the density of fluid, $\rho = \rho_f n + \rho_s (1 - n)$ is the average density of porous seabed (ρ_s is solid density), u , v and w are the soil displacements in the x -, y - and z -direction, respectively, σ'_x , σ'_y and σ'_z are the effective normal stresses in the x -, y - and z -direction, respectively, τ_{xy} , τ_{yz} and τ_{zx} are shear stresses, ϵ_s is the volume strain of soil matrix which is defined as

$$\epsilon_s = \frac{\partial u}{\partial x} + \frac{\partial v}{\partial y} + \frac{\partial w}{\partial z} \quad (12)$$

where β is the compressibility of the pore fluid, which is related to the apparent bulk modulus of the pore fluid K' and the degree of saturation S_r , such that

$$\beta = \frac{1}{K'} = \frac{1}{K_w} + \frac{1 - S_r}{P_{w0}} \quad (13)$$

where K_w is the bulk modulus of pore water ($K_w = 2 \times 10^9 \text{ N/m}^2$), P_{w0} is the absolute water pressure.

$$\sigma'_x = 2G \left[\frac{\partial u}{\partial x} + \frac{\mu}{1 - 2\mu} \epsilon_s \right] \quad (14)$$

$$\sigma'_y = 2G \left[\frac{\partial v}{\partial y} + \frac{\mu}{1 - 2\mu} \epsilon_s \right] \quad (15)$$

$$\sigma'_z = 2G \left[\frac{\partial w}{\partial z} + \frac{\mu}{1 - 2\mu} \epsilon_s \right] \quad (16)$$

$$\tau_{xz} = G \left[\frac{\partial u}{\partial z} + \frac{\partial w}{\partial x} \right] = \tau_{zx} \quad (17)$$

$$\tau_{yz} = G \left[\frac{\partial v}{\partial z} + \frac{\partial w}{\partial y} \right] = \tau_{zy} \quad (18)$$

$$\tau_{xy} = G \left[\frac{\partial u}{\partial y} + \frac{\partial v}{\partial x} \right] = \tau_{yx} \quad (19)$$

where the shear modulus G is related to Young's modulus E by the Poisson's ratio μ in the form of $E/A(1 + \mu)$. Substituting Eqs. (14)–(19) into (9)–(11), the equations of force equilibrium become (9)–(11) in the x -, y - and z -directions, respectively.

$$G \nabla^2 u + \frac{G}{(1 - 2\mu)} \frac{\partial \epsilon_s}{\partial x} = \frac{\partial p}{\partial x} + \rho \frac{\partial^2 u}{\partial t^2} \quad (20)$$

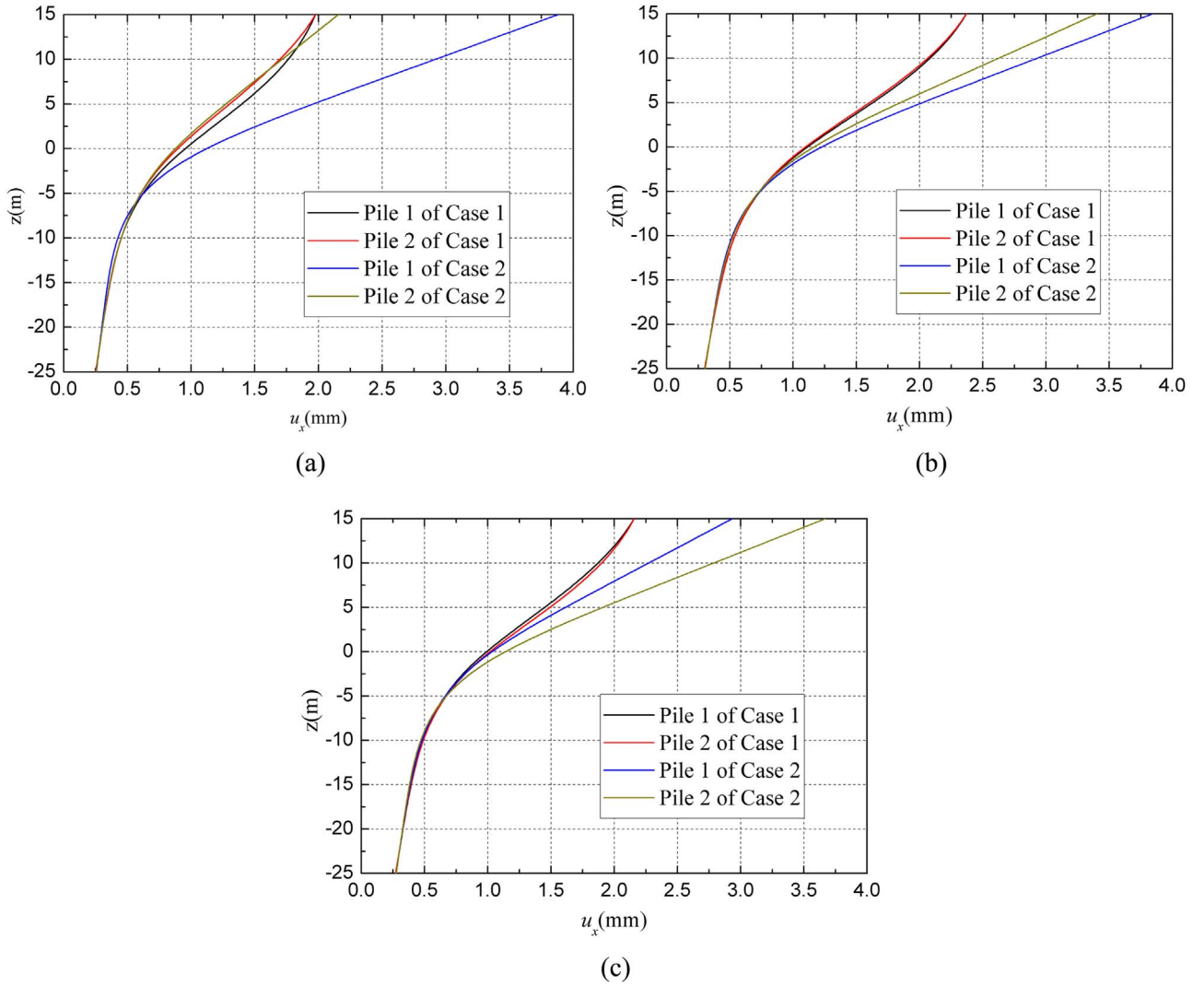


Fig. 8. Distribution of displacement of pile along depth z when the wave crest at the position (a) Pile 1; (b) mid-position; (c) Pile 2 for Case 1: pile foundation with platform; Case 2: pile foundation without platform.

$$G\nabla^2 v + \frac{G}{(1 - 2\mu)} \frac{\partial \epsilon_s}{\partial y} = \frac{\partial p}{\partial y} + \rho \frac{\partial^2 v}{\partial t^2} \tag{21}$$

$$G\nabla^2 w + \frac{G}{(1 - 2\mu)} \frac{\partial \epsilon_s}{\partial z} = \frac{\partial p}{\partial z} + \rho \frac{\partial^2 w}{\partial t^2} \tag{22}$$

3. Boundary conditions

3.1. Boundary Equation of Wave

As shown in Fig. 1, appropriate boundary conditions are required to solve the VARANS governing equations to the wave sub-model. A periodic, linear, surface wave generated for the investigation based on the assumptions that the fluid is incompressible and inviscid, and the wave amplitude is small compared to the mean water depth and wavelength. Therefore, the free surface elevation $\eta(x, t)$ measured in the vertical direction from mean water surface can be written as

$$\eta = A \cos(k'x - \omega t + \phi) \tag{23}$$

where A is the wave amplitude, $k' = 2\pi/L$ is the wave number, ω is the

angular frequency, ϕ is the phase shift, and t is time.

The outflow boundary is applied at the outlet area, which is a radiation boundary condition, to avoid the reflection of wave. The numerical model is not limited by physical dimensions, therefore, it can imagine that there is a mathematical continuation of the flow beyond the end of the computed region. This is the essence of the Sommerfeld radiation boundary condition, which in fact is a simple mathematical continuation having the form of outgoing waves (Orlanski, 1976)

$$\frac{\partial Q}{\partial t} + c \frac{\partial Q}{\partial x} = 0 \tag{24}$$

where Q is any quantity, positive x is directed out of the boundary, and c is the local phase speed of the flow.

The pressure of the free water surface is considered to be the standard atmospheric pressure ($p = p_a$), and the gradient of velocity components are zero in the normal direction of the free surface. On the water-pile interface, no-slip boundary is given and the turbulence properties are estimated from law of the wall boundary condition. The velocity of the fluid in the normal vector is zero at the bottom, and the flow rate and the fluid shear stress are zero at the sides on the other hand. The Symmetry boundary condition is adopted at the two sides of

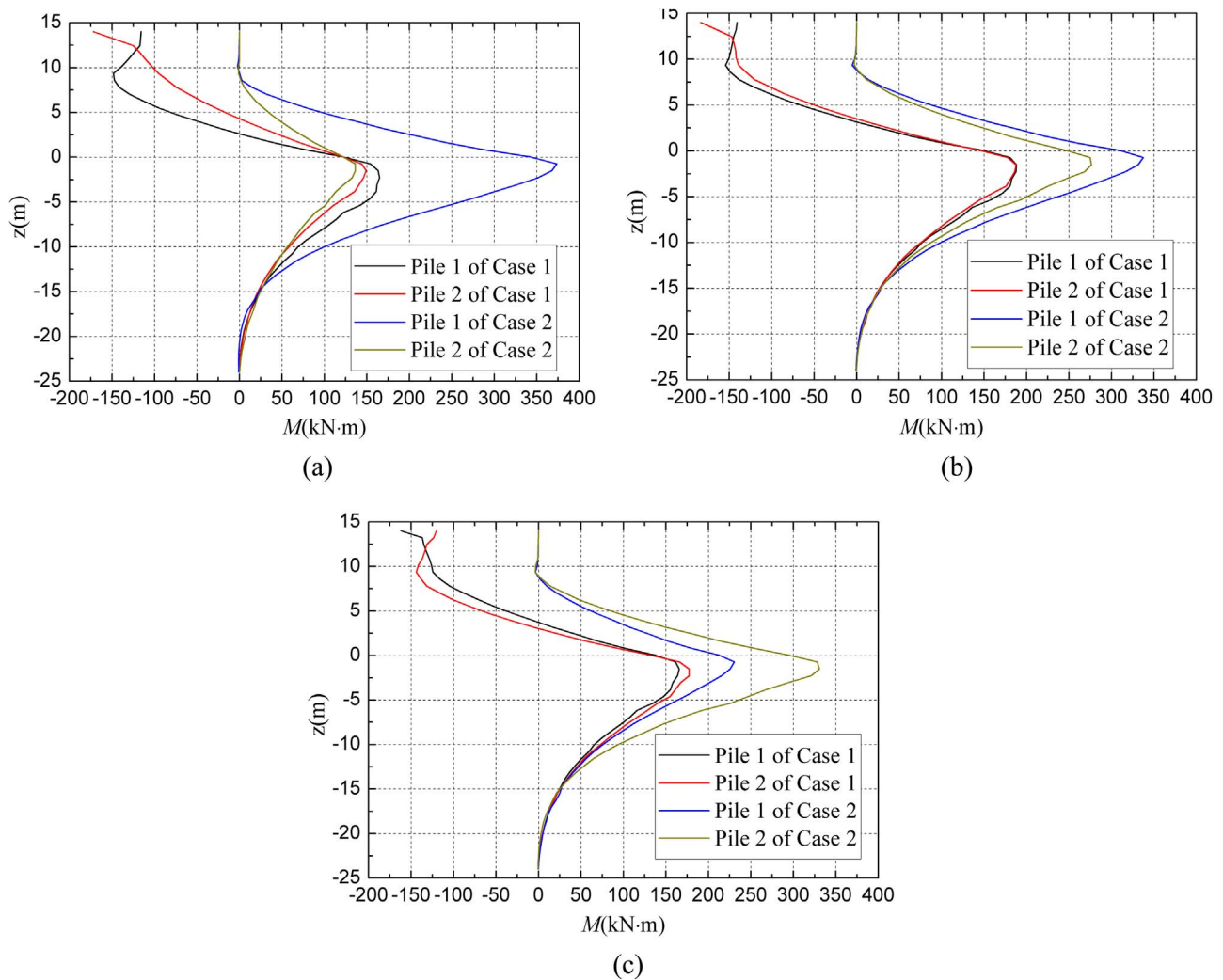


Fig. 9. Distribution of bending moment of pile along depth z when the wave crest at the position (a) Pile 1; (b) mid-position; (c) Pile 2 for Case 1: pile foundation with platform; Case 2: pile foundation without platform.

the wave model, as a result, the wave can slide freely along the boundary but cannot penetrate nor pull away. The Wall boundary is applied at the bottom of the model to simulate the seabed surface.

3.2. Boundary condition of seabed

To the seabed sub-model, appropriate boundary conditions are also required to solve the governing Eqs. (20)–(22) which mainly evaluating the wave-induced seabed response. Therefore, the boundary conditions can be divided into the following sections.

3.2.1. Boundary condition at the seabed surface

It is commonly accepted that the vertical effective stress and shear stress vanish when the viscosity and friction of water is ignored in a porous seabed of finite thickness. The pore pressure p is equal to the wave pressure p_b obtained from the wave sub-model.

$$\sigma'_z = \tau_{zx} = \tau_{zy} = 0; \quad p = p_b \text{ at } z = 0 \quad (25)$$

3.2.2. Boundary condition at the seabed bottom

Based on a proper computing domain of the seabed sub-model which is sufficient to avoid the influence of the boundary conditions, the seabed bottom is treated as impermeable and rigid. Therefore, there is no displacement and vertical flow occur in this boundary.

$$u = v = w = \frac{\partial p}{\partial z} = 0 \text{ at } z = h \quad (26)$$

3.2.3. Boundary condition at the seabed four vertical sides

The four vertical sides of the seabed are considered as impermeable. This means that zero soil displacement and flow occur in the x -direction of the left and right sides, the same as the y -direction of the front and back sides.

$$u = \frac{\partial p}{\partial x} = 0 \text{ at } x = \pm \frac{a_0}{2} \quad (27)$$

$$v = \frac{\partial p}{\partial y} = 0 \text{ at } y = \pm \frac{b_0}{2} \quad (28)$$

in which a_0 and b_0 are the length and width of the wave sub-model.

3.2.4. Boundary condition of pile foundation

There is no flow through the pile surface due to the interface between the pile foundation and the porous seabed is considered as impermeable. Therefore, the pore gradient on the surface of the pile foundation should vanish.

$$\frac{\partial p}{\partial n} = 0 \text{ at } r = \sqrt{(x - x_i)^2 + (y - y_i)^2} = \frac{D}{2}; \quad z \in [0, h] \quad (29)$$

where x_i and y_i donate the coordinates of the center of each pile

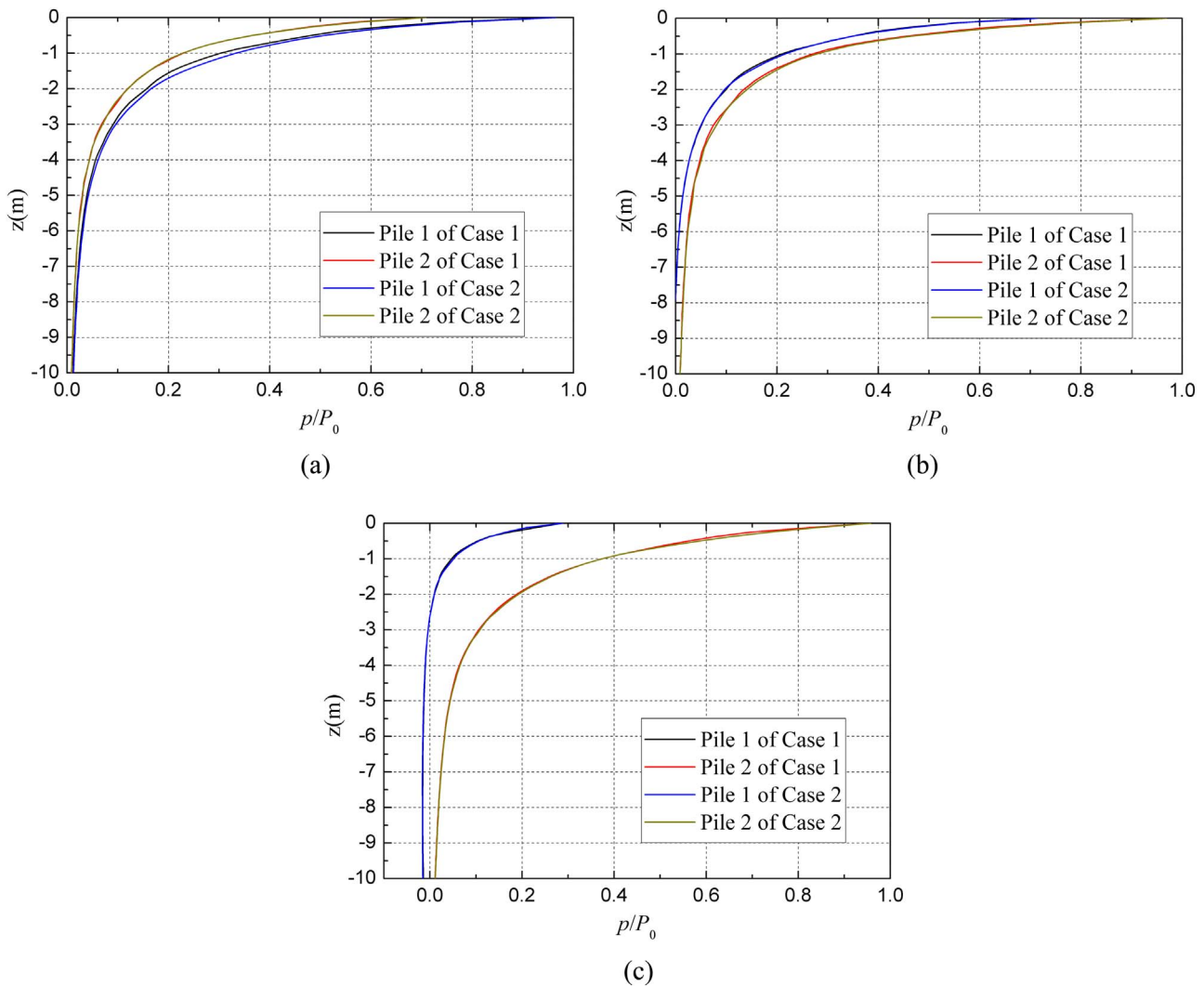


Fig. 10. Distribution of pore pressure around pile along depth z when the wave crest at the position (a) Pile 1; (b) mid-position; (c) Pile 2 for Case 1: pile foundation with platform; Case 2: pile foundation without platform.

($i=1,2,3,4$), n is the normal direction to the surface of the pile, and D is the pile diameter.

4. Numerical methods

As mentioned before (Fig. 1), the proposed integrated numerical model is divided into two sub-models: the wave sub-model and seabed sub-model. Although the whole model is divided into two parts, they are closely related in the process of integrating the VARANS equations and dynamic Biot's equation.

4.1. Wave sub-model

To the wave save sub-model, the VARANS governing equations are solved to obtain the wave forces on the pile foundation platform, and the impact of wave motion on seabed response is imposed on the sea floor in the form of wave pressure p_b . The finite difference two-step projection method on a staggered grid system is adopted for the space discretization, and time derivative is discretized by the forward time difference method. The VOF method (Hirt and Nichols, 1981) and the Fractional Area/Volume Obstacle Representation (FAVOR) method (Hirt and Sicilian, 1985) are used to track the free water surface, which consists of three main components: the definition of the volume of fluid function, a method to solve the VOF transport equation and setting the

boundary conditions at the free surface. The idea of VOF method is to define a function F to represent the fractional volume water fluid

$$\frac{\partial F}{\partial t} + \frac{\partial(u_i F)}{\partial x_i} = 0 \tag{30}$$

where $F = 0$ indicates that the cell is full of air, and $F = 1$ indicates that the cell is full of water. The piecewise linear interface calculation (PLIC) method (Kothe and Rider, 1998) is applied to reconstruct the air-water interface.

In the wave sub-model, we consider a pile foundation platform in a numerical wave tank with the scale of 230 m long, 30 m wide, and 16.5 m high (see Fig. 2a). The pile foundation platform is placed 80 m from the wave inlet boundary to provide sufficient length for the waves to propagate. The pile foundation surface is treated as no-slip boundary and the turbulence properties are estimated from law of the wall boundary condition. The mesh used in this simulation is composed of two partially overlapping mesh blocks to ensure the accuracy of numerical modeling: a mesh block 1 that used to define the whole simulation regions with 117,300 cells, and a mesh block 2 with 396,000 cells that are finer closed to the structure. Furthermore, the time interval is automatically adjusted at each time step to satisfy Courant-Friedrichs-Lewy condition and the diffusive limit condition (Sanz-Serna and Spijker, 1986).

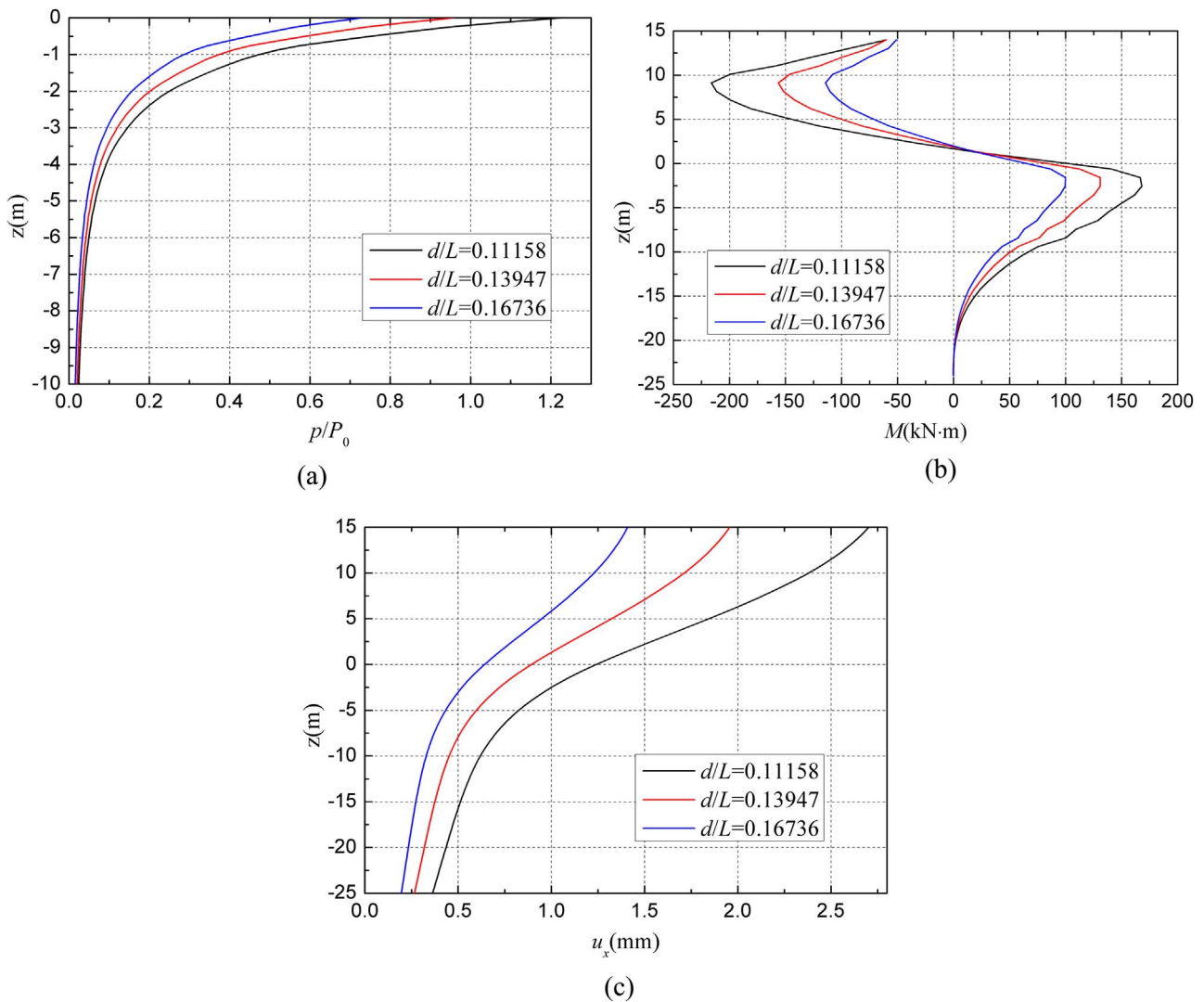


Fig. 11. Distribution of (a) pore pressure along depth z ; (b) bending moment along depth z ; (c) displacement along depth z for various water depth.

4.2. Seabed sub-model

In order to solve the Biot's u - p equations to obtain response of the seabed and structure, FEM (Finite Element Model) codes are constructed within the COMSOL Multiphysics, by designing user's own governing equations and boundary conditions in a certain physical model. As shown in Fig. 2, the seabed sub-model configuration is 100 m×40 m×30 m. The system is discretized into unstructured Lagrange elements with a maximum global element size of 2 m, meanwhile the local refinement of mesh has been taken into account in the regions near the pile foundation with a maximum element size of 0.5 m, which could obtained more detailed expected results in these regions.

4.3. Integration of wave and seabed models

In the integrated model, the wave sub-model is responsible for the simulation of the wave propagation and determines the pressure acting on the porous seabed and piles, and the seabed sub-model is responsible for the calculation of the wave-induced seabed response and the dynamic response of pile foundation platform. So that a data exchange port is required to combine the two sub-models together at the interface between the wave sub-model and the seabed sub-model. As a result, the wave pressure and forces acting on the porous seabed and pile foundation determined by the wave sub-model are provided to

the seabed sub-model through the data exchange port developed to calculate the dynamic response of the seabed and pile foundation, including the pore pressure of the seabed, the displacements and the bending moments of pile foundation. The details of the process are illustrated in Fig. 3.

5. Numerical results and discussion

In marine environment, the existence of pile foundation platform will change the equilibrium of the flow field, and the interaction of pile group make the situation more complex under regular waves. The effects of pile group foundation are mainly caused by the phase difference of each piles, which are due to the influence of the wave height (h), wavelength (L) and pile spacing (l), and the disturbance of the flow field. Additionally, the mechanical behavior of pile foundation platform is much more different than the structure without platform. To a pile foundation without platform, each pile is just subject to the wave force and without other forces or restrictions. However, a pile foundation platform is not just under the wave force, but also subject to the restraint of the platform. Therefore, the main objective of this study is to investigate the wave-induced seabed response around the pile foundation platform. In this section, to validate the proposed numerical model, we firstly compare the present results with the experimental data and the analytical results.

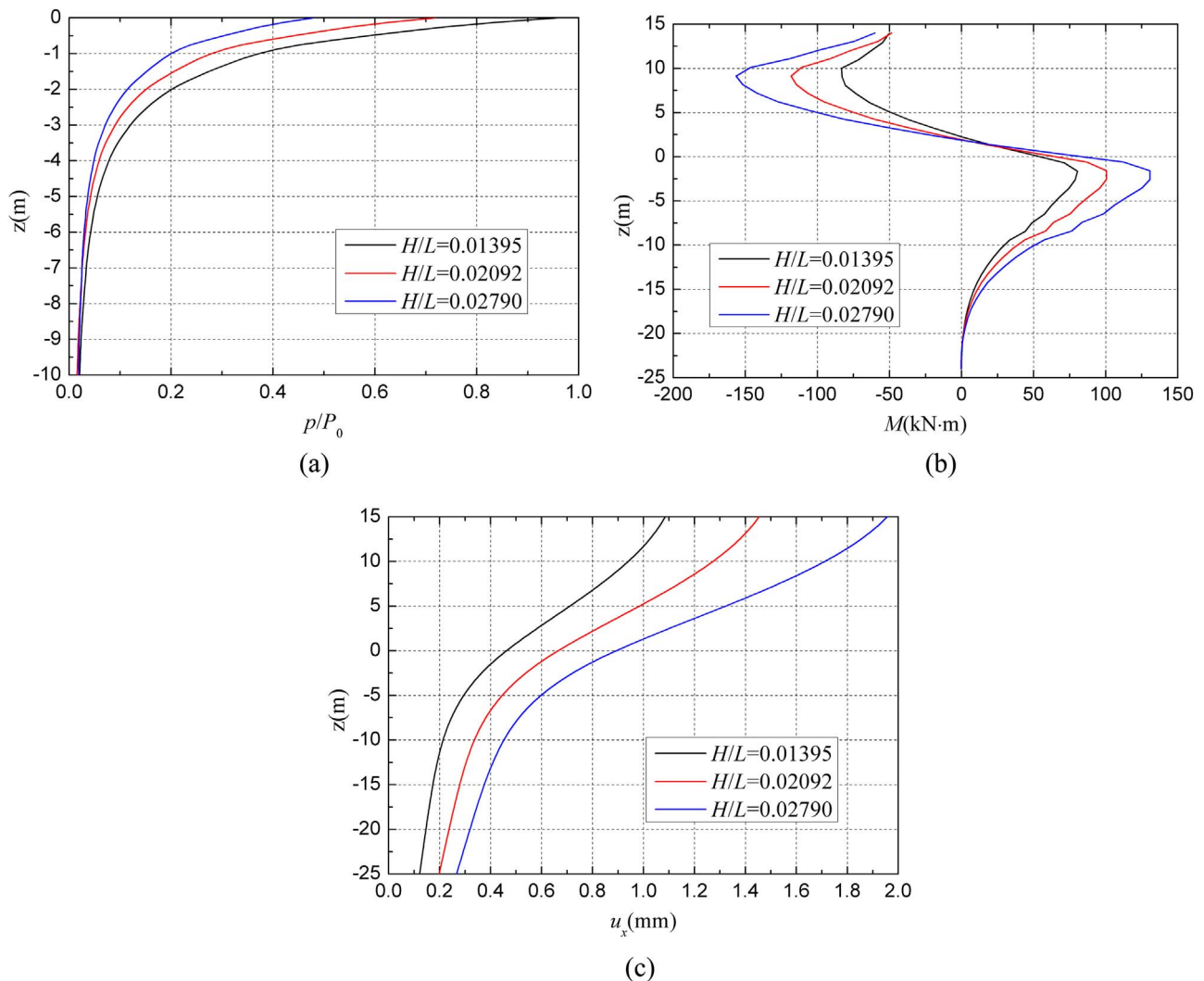


Fig. 12. Distribution of (a) pore pressure along depth z ; (b) bending moment along depth z ; (c) displacement along depth z for various wave height.

5.1. Verification of the present model

Firstly, in order to verify the accuracy of the numerical model, the present results for the porous seabed response without pile foundation due to linear wave are compared with the previous results (Hsu and Jeng, 1994), which parameters are based on the design wave condition of North Sea, China. The input data for the comparison are tabulated in Table 1. As a result, the free surface profile of the linear wave generated from the present model is compared with the theoretical solution, as shown in Fig. 4, in which the black dots denotes the numerical result of the present model, and the solid line represent the theoretical solution. It is clearly that the numerical result of the free surface based on the wave sub-model agrees very well with the theoretical solution.

Moreover, Fig. 5 illustrates the comparison of p/P_0 , $|\sigma'_x|/P_0$ and $|\sigma'_z|/P_0$ between the present results and Hsu and Jeng (1994) base on the seabed sub-model, where the points represent the previous results from Hsu and Jeng (1994), and the solid lines represents the present results. The solution of Hsu and Jeng (1994) did not consider inertia effects, which was Quasi-Static model (Biot's consolidation equations). In this paper, we adopted so-called u - p model, which was consider inertia effects. The parameter P_0 is the amplitude of wave pressure for a linear wave, which also can be given by the equation

$$P_0 = \frac{\rho_w g H}{2 \cosh k'd} \quad (31)$$

where k' is the wave number. The numerical results shown that the relative difference between the u - p solution (with inertia items) and the Quasi-Static solution (without inertia items) may reach 4% under certain combinations of wave and soil conditions. This phenomenon was reasonable. The numerical results of Jeng et al. (1999) showed that the inertia forces cannot always be ignored in a softer seabed. The relative difference between the u - p solution (with inertia items) and the Quasi-Static solution (without inertia items) may reach 5% under certain combinations of wave and soil conditions.

5.2. Effect of pile foundation on the distribution of flow field

5.2.1. Flow field around pile foundation in one period

Fig. 6 illustrates the vector fields and the distribution of the wave pressure around the 2×2 array of piles at the depth $z = 0.35$ m in one wave period, where the wave pressure variation is represented by the color images, the velocity vector is donated by the black arrow, and the black line is the contour plots of the free surface elevation. The input data which used from the standard model parameters are listed in Table 2, where the non-dimensional pile spacing $l_p/D = 2$. Note that the pile spacing is quite small relative to the wave length, therefore the

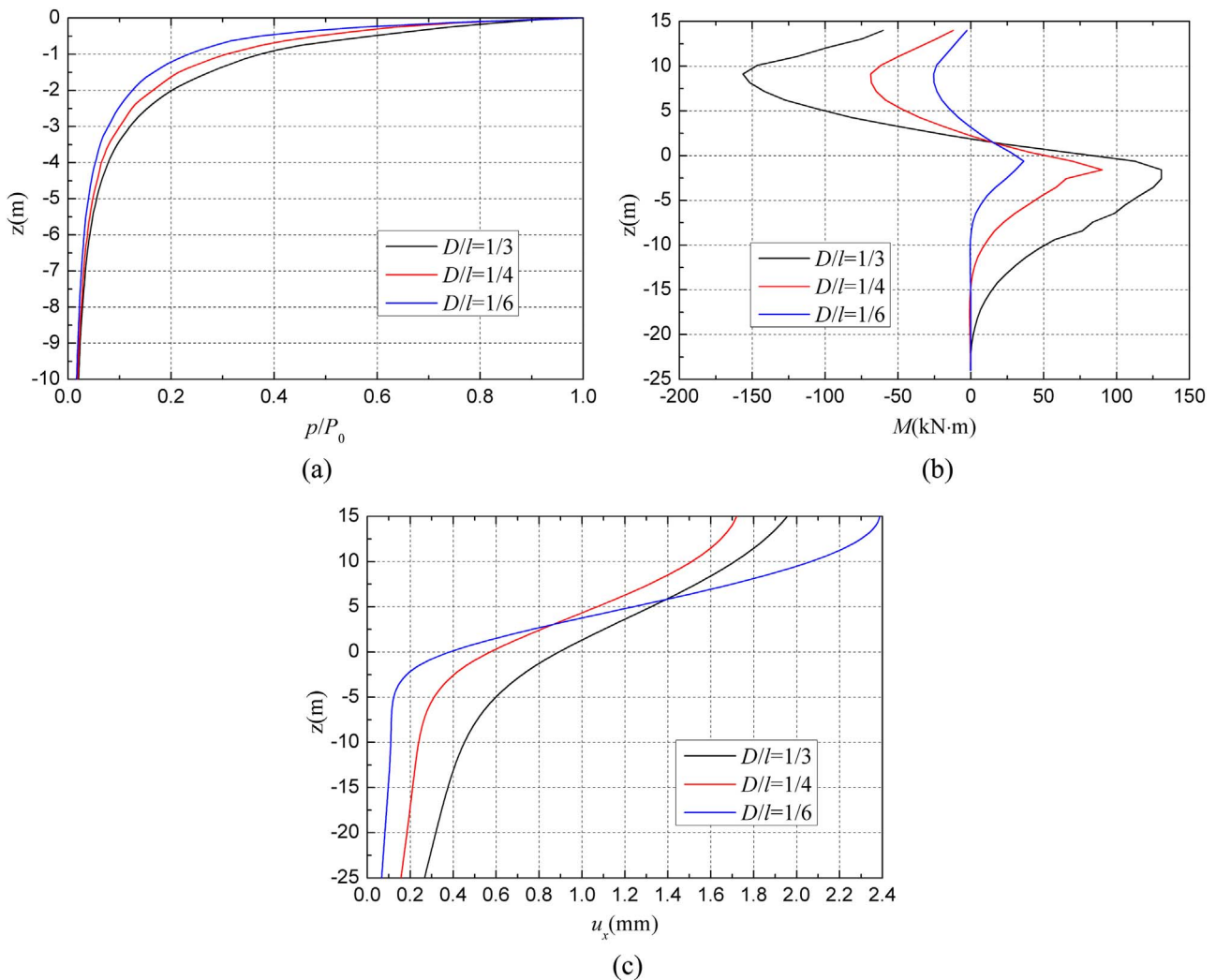


Fig. 13. Distribution of (a) pore pressure along depth z ; (b) bending moment along depth z ; (c) displacement along depth z for various pile diameter.

wave crest or trough could not pass the upstream piles and the downstream piles simultaneously, and it is obvious that the flow field is almost symmetrically between Pile 1, 2 and Pile 3, 4 in the wave direction.

When the wave crest occurs on Pile 1 (Fig. 6a), the crest height is increased in front of Pile 1 which leads to a large net difference in the pressure around Pile 1. As a result, Pile 1 reaches the maximum positive velocity. Water on the windward side of Pile 1 is obstructed and the waves flow to the lateral sides of the pile, then converge on its leeward side. This generates a high speed zone and a low speed zone on the windward side and leeward side of Pile 1, separately. Meanwhile, the wave trough passes the Pile 2 after finishes its motion in the negative x -direction, which leads to a low speed zone around Pile 2. It is worth noting that the waves are obstructed and pushed sideways on the leeward side of Pile 2 before the waves converge completely on the leeward side of Pile 1, and the main reason is that because of the pile spacing is not long enough for the waves return to the x -direction between the two piles. When the wave crest reaches to Pile 2, as shown in Fig. 6b, it can be clearly seen that the waves scatter on the windward side and then converge on the leeward side, which is almost same to the phenomenon when the wave crest occurs on Pile 1. However, due to the shadowing of the waves by Pile 1, Pile 2 experiences a lower pressure and velocity on the windward side, compared with the results of Pile 1 when the wave crest reaches it.

When Pile 1 or 2 are at the equilibrium position between the wave crest and trough (Fig. 6c and d), the wave crest just finishes its motion in the positive x -direction, but the wave trough not reached to the pile yet. Therefore, it can be clearly seen that there exists a low speed zone around the pile, which is due to the velocities of the windward side and leeward side are in opposite directions. When the wave trough reaches to Pile 1 or 2 (Fig. 6e and f), it reaches its maximum velocity in the negative x -direction. The vector field and the distribution of wave pressure are similar to the situation when the wave crest reaches, except the direction of velocity and the value of wave pressure.

5.2.2. Effect of non-dimensional pile spacing

As discussed before, the non-dimensional pile spacing l_p/D has a significant effect on the wave propagation. Therefore, the effect of l_p/D to the flow field is discussed here. Fig. 7 illustrates the velocity vector and the distribution of the wave pressure around the 2×2 array of pile foundation at the water depth $z = 0.35$ m, and the non-dimensional pile spacing l_p/D equals to 2, 3 and 4, respectively.

From the numerical results represented in Fig. 7, the differences of wave velocity vector between these three cases are significant. When l_p/D equals to 4, after the waves scatter on the windward side and converge on the leeward side of Pile 1, the waves return to the horizontal direction and keep a visible distance in the mid-position between Pile 1 and Pile 2, then reach to Pile 2. Therefore, the existence of

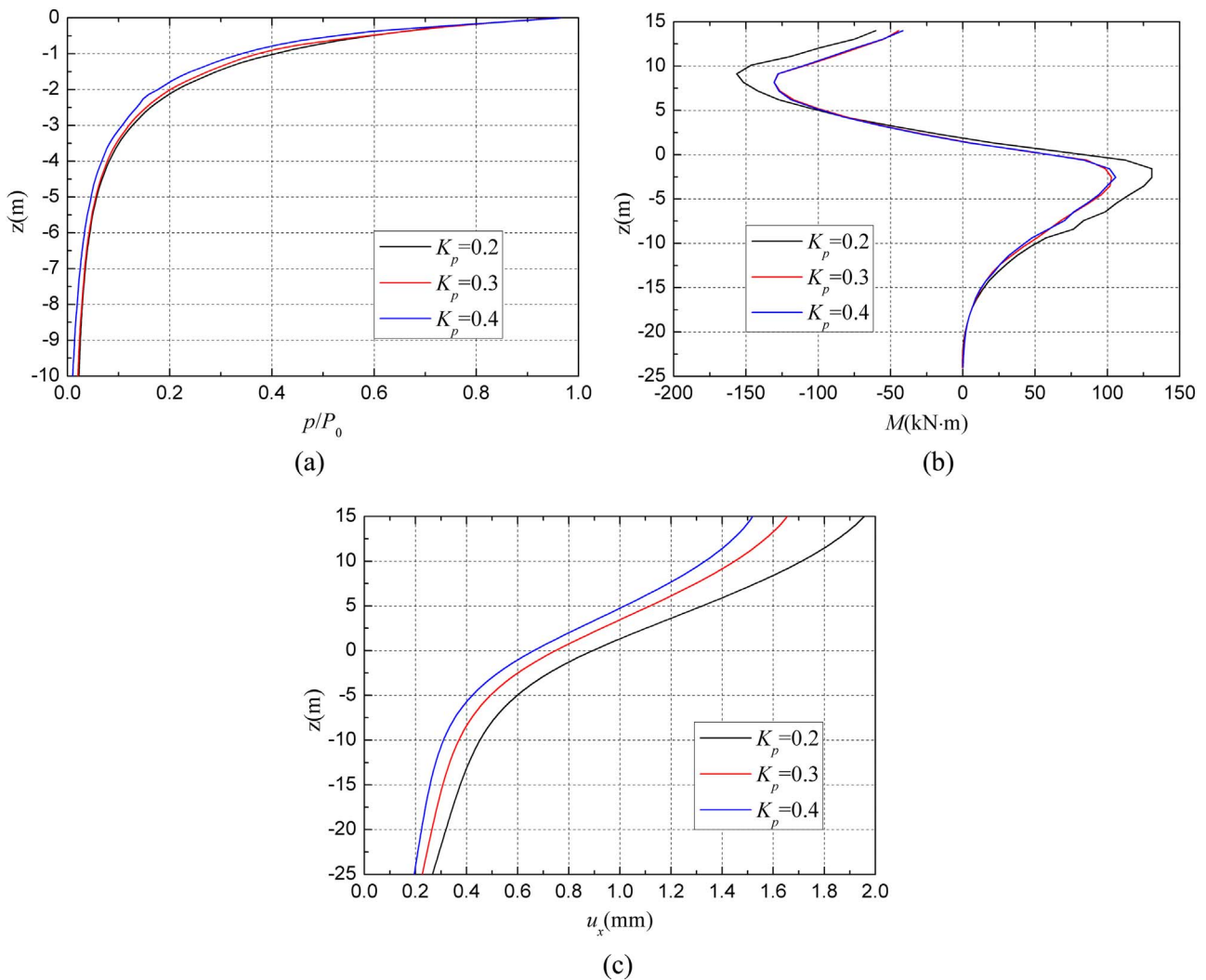


Fig. 14. Distribution of (a) pore pressure along depth z ; (b) bending moment along depth z ; (c) displacement along depth z for various pile insertion ratio.

Pile 1 has little shadowing effect to Pile 2, and the values of velocity equal to 1.38 m/s at the time instant when the wave crest reaches to Pile 1 and Pile 2. When l_p/D equals to 3, water on the windward side of Pile 2 is obstructed and then pushed sideways immediately after the waves converge on the leeward side of Pile 1, it almost cannot observe the waves return to the x -direction between Pile 1 and 2. Meanwhile, the wave velocity equal to 1.37 m/s and 1.35 m/s when the wave crest reach to Pile 1 and Pile 2, separately. When l_p/D equals to 2, the existence of Pile 1 have evident shadowing effect to the vector field of Pile 2, as what has been mentioned in the above section, and the wave velocity reduces from 1.35 m/s to 1.32 m/s, with a decrease of 0.03 m/s. In general, the numerical results show that the non-dimensional pile spacing affects evidently on the flow field, the shadowing effect decreases with the non-dimensional pile spacing l_p/D increases, and the shadowing effect almost disappear when $l_p/D \geq 4$.

5.3. Effect of the existence of platform

For the reason that there is a phase difference between Pile 1 and Pile 2, the wave crest cannot reach to Pile 1 and Pile 2 at the same time, and the existence of the rigid platform makes the situation more complicated. In this section, the pile foundation with platform and without platform are established separately to investigate the displacement and bending moment of the piles and the pore pressure around

the piles, where the input data are listed in Table 2, notice that the non-dimensional pile spacing $l_p/D = 3$ in this section. Figs. 8–10 illustrate the distributions of displacement u_x , bending moment M of Pile and pore pressure p/P_0 along depth z when the wave crest at the position (a) Pile 1; (b) mid-position; (c) Pile 2 for Case 1 (pile foundation with platform) and Case 2 (pile foundation without platform). The difference between Case 1 and Case 2 is significant, and the results of Pile 1 and Pile 2 are different at the same time due to the phase difference. As shown in Fig. 8, the displacement u_x decreases rapidly with the decrease of the pile depth of the pile foundation without platform.

The maximum value of u_x appears at the pile head, where the values of u_x of Pile 1 and Pile 2 are 3.88 mm and 2.16 mm, 3.84 mm and 3.40 mm, 2.93 mm and 3.67 mm, respectively, at the time instant when the wave crest reaches to Pile 1, the mid-position between Pile 1 and Pile 2, and Pile 2 (Fig. 8). It can be seen that the maximum u_x of Pile 1, which equals to 3.88 mm, is greater than Pile 2 that equals to 3.67 mm due to the shadowing effect. Moreover, the effect of platform is significant. Pile 1 and Pile 2 have the same displacements at pile head because of the effects of the platform, and the displacement u_x reduces dramatically to a maximum value of 2.37 mm when the wave crest reaches to the mid-position, the maximum displacements u_x are 1.98 mm and 2.16 mm respectively when the wave crest reaches to Pile 1 and Pile 2.

The maximum bending moment of the pile foundation without

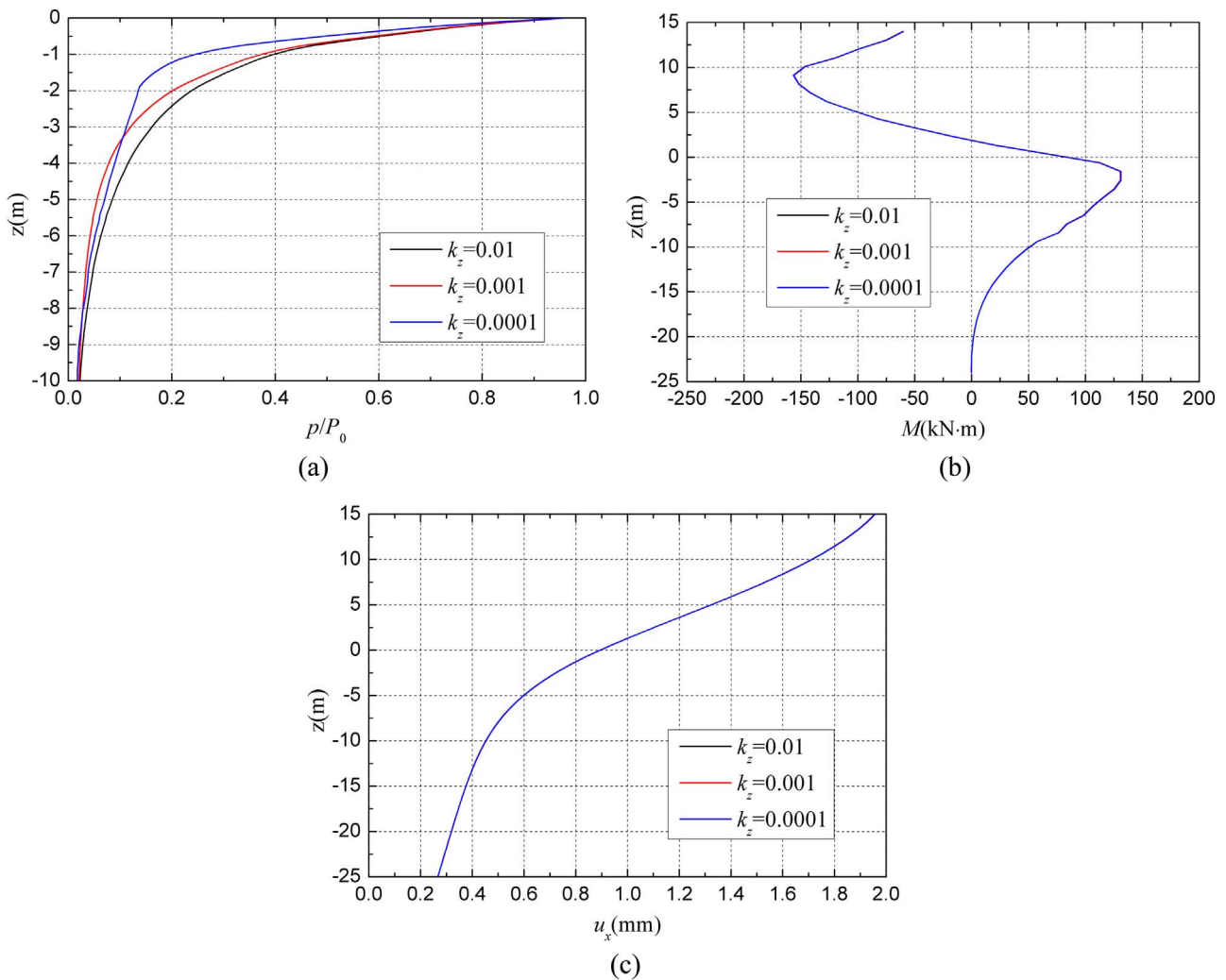


Fig. 15. Distribution of (a) pore pressure along depth z ; (b) bending moment along depth z ; (c) displacement along depth z for various seabed permeability.

platform appears near the height $z = -1.5$ m, and the maximum value equals to 373.74 kN m at the time instant when the wave crest reaches to Pile 1, which is greater than the value of Pile 2 that equals to 330.60 kN m at the time instant when the wave crest reaches it (Fig. 9). The values of bending moments M at pile head and bottom are zero. Whereas, the existence of the platform changes the distribution of M and reduces the maximum value to 188.04 kN m at the position $z = -1.5$ m. It is worth noticing that the negative bending moments show up at the pile head due to the restraint of the platform, and the bending moment are different near the area of the pile head.

As to the pore pressure, there is no much difference whether the platform exists or not (Fig. 10). The pore pressure decreases in vertical direction from the seabed surface, and the value is close to zero at the position $z = -10$ m. However, the pore pressure is different between Pile 1 and Pile 2 due to the phase difference.

5.4. Effects of wave, pile and seabed parameters

5.4.1. Effects of wave characteristics

In this section, the effects of wave major parameters including wave depth and wave height are discussed to investigate the wave-induced seabed and pile foundation platform response. Fig. 11 illustrates the distribution of u_x , M and p/P_0 of Pile 1 for three relative depth d/L ($d/L = 0.11158, 0.13947, 0.16736$), the other input data being listed in Table 2. It is clearly found that the pore pressure p/P_0 decreases as the relative depth d/L increases (Fig. 11a) near the seabed surface, and

both of these three cases reduce along the vertical direction have the same change tendency. The bending moment M of the pile increases as the relative depth d/L decreases, and the maximum M appears at the same position of the three cases, in which the positive maximum value appears at the position $z = -2.5$ m, and the negative maximum value appears at the position $z = 9$ m (Fig. 11b). As shown in Fig. 11c, the displacement u_x of the pile increases as the relative depth d/L decreases.

Fig. 12 illustrates the distributions of the displacement, bending moment and pore pressure with various relative wave height H/L ($H/L = 0.01395, 0.02092, 0.02790$). It can be seen that both of p/P_0 , u_x and M increase as the wave height H/L increases, and the distributions of p/P_0 , u_x and M along the vertical direction have the same trend with the results of d/L . The results show that the relative depth d/L and the relative wave height H/L have significant effects on the wave-induced seabed and pile foundation platform response.

5.4.2. Effects of pile characteristics

Pile characteristics play an important role in the dynamic response of the seabed and structure under wave loading, where the relative pile diameter D/l and pile insertion ratio K_p ($K_p = d_{pw}/d_{ps}$, where d_{pw} is the pile length above the mudline and d_{ps} is the pile length below the mudline, $d_p = d_{pw} + d_{ps}$ is the whole length of the pile) are the main factors. The vertical distributions of the wave-induced pore pressure of seabed, displacement and bending moment of Pile 1 for various values of relative pile diameter $D/l = 1/3, 1/4, 1/6$ are plotted in Fig. 13. It is

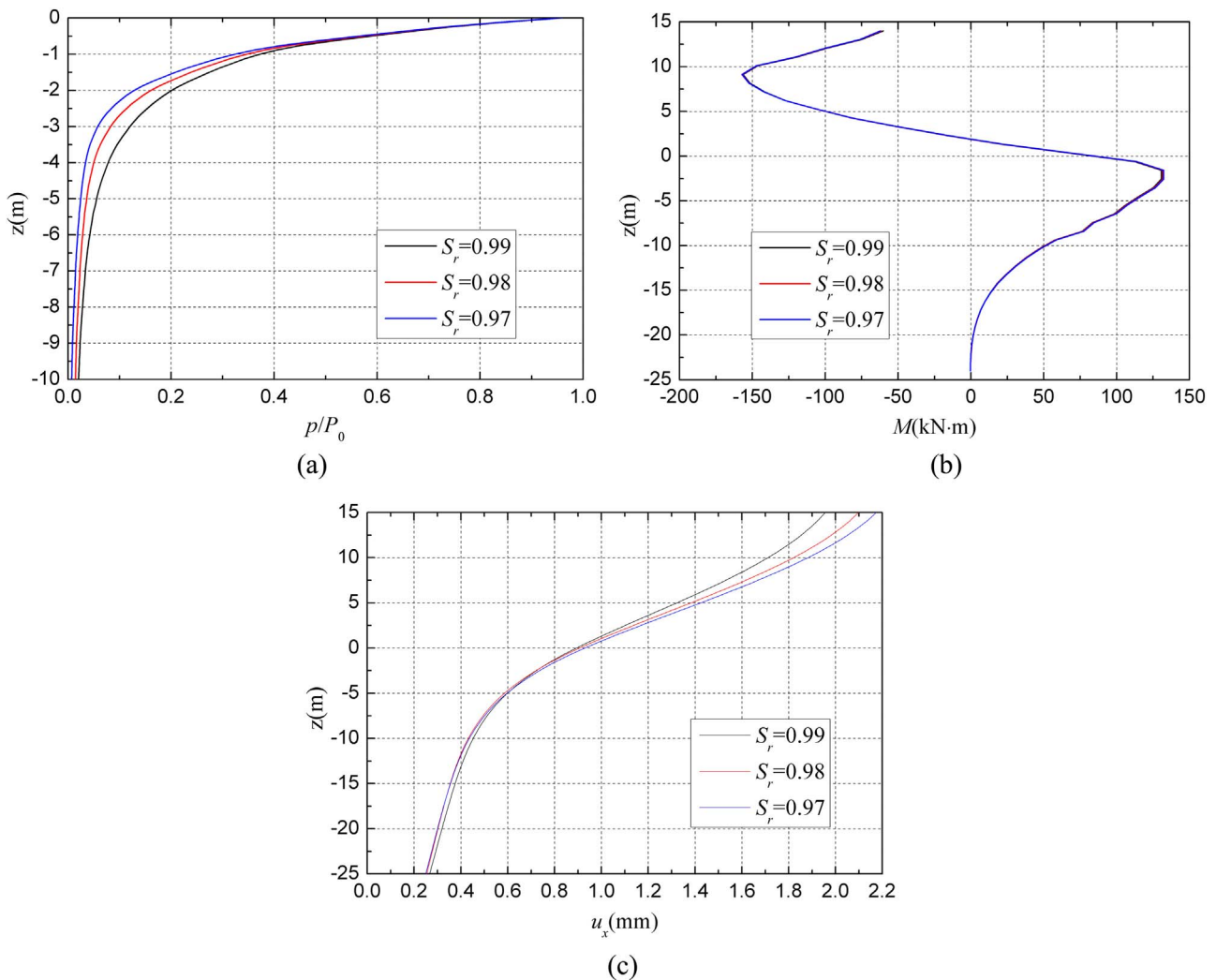


Fig. 16. Distribution of (a) pore pressure along depth z ; (b) bending moment along depth z ; (c) displacement along depth z for various degree of saturation.

found that p/P_0 has little difference near the seabed surface for various relative pile diameter D/l , but the pore pressure decreases rapidly as the relative pile diameter D/l decreases. The bending moment of pile decreases as the relative pile diameter D/l decreases (Fig. 13b), which is related to the magnitude and distribution of the wave force on the pile. Fig. 13c shows that the displacement of pile decreases as the relative pile diameter D/l decreases. However, when the relative pile diameter D/l equals to $1/6$, the maximum value of u_x is greater than the other cases at pile head, and the displacement reduces more rapidly along the vertical direction of the pile foundation, which is mainly due to a small pile stiffness when D/l equals to $1/6$.

Fig. 14 presents the distribution of the wave-induced pore pressure, displacement and bending moment of the pile for various pile insertion ratio $K_p = 0.2, 0.3, 0.4$. The results show that the pore pressure increases slightly as K_p decreases. The bending moment of pile decreases as the pile insertion ratio K_p decreases to the value of 0.3, but the bending moment almost has no reduction from the case $K_p = 0.3$ to $K_p = 0.2$. The same law is also found in the distribution of the displacement of pile: the displacement of pile decreases as the pile insertion ratio K_p decreases, it is worth noting that the reduction of the displacement of pile from the pile insertion ratio $K_p = 0.3$ to $K_p = 0.2$ is much less than from $K_p = 0.4$ to $K_p = 0.3$. This indicated that the

influence of pile insertion ratio on the displacement of pile decreases gradually with the pile insertion ratio increases.

5.4.3. Effects of seabed characteristics

Meanwhile, the seabed characteristics are also important parameters in determining the wave-induced seabed and pile foundation platform response. In this section, the soil permeability k_z , which is an indication of the ability for fluids to flow through soil skeleton that related to the porosity and the density and viscosity of fluid, and the degree of saturation S_r ($S_r = V_w/V_v$, where V_w is the volume of water and V_v is the volume of pore space) are selected for the investigation. Considering three kind of seabed permeability (Case 1: coarse sand, $k_z = 1.0 \times 10^{-2}$ m/s; Case 2: intermediate sand, $k_z = 1.0 \times 10^{-3}$ m/s; and Case 3: fine sand, $k_z = 1.0 \times 10^{-4}$ m/s), the other parameters are listed in Table 2. As shown in Fig. 15a, the pore pressure increases as the permeability k_z increases. For instance, the pore pressure attenuates rapidly near the seabed surface when $k_z = 1.0 \times 10^{-4}$ m/s, and the attenuation of velocity slows down at the position $z = -2$ m. On the other hand, the pore pressure p/P_0 attenuates slowly along seabed depth for Case 1 with the permeability $k_z = 1.0 \times 10^{-2}$ m/s. Fig. 15b and c illustrate the distributions of the displacement and bending moment of Pile 1 for various seabed permeability. It is found that with the

change of k_z , there is no difference for either the displacement or the bending moment of the pile.

The distribution of the pore pressure, displacement and bending moment of Pile 1 for various degree of saturation $S_r = 0.99, 0.98, 0.97$ are plotted in Fig. 16. It can be found that the pore pressure p/P_0 increases as the degree of saturation increases. The bending moment of pile has little difference between the three cases. However, the distributions of the displacement with different values of S_r are slightly different, as shown in Fig. 15c. The displacement decreases rapidly for $S_r = 0.99$ than that for $S_r = 0.98$ and 0.97 , and the displacement of the three cases have the same value at the position $z = -2.5$ m. The above results indicate that k_z and S_r have clear effects on the distributions of pore pressure, but almost have no effects on the distributions of displacement and bending moment of the pile.

6. Conclusion

In this study, the numerical model has been developed to investigate the problem of wave-seabed-pile foundation platform system interaction based on wave and seabed sub-models. The VARANS equations govern the wave sub-models and the Biot's theory (u - p model) describes the seabed sub-model and pile foundation platform under wave loading. Good agreement of the results show that the numerical model is effective for the investigation. Based on the numerical results presented, the following conclusions can be obtained:

- (1) The phenomenon of wave diffraction around the array of pile foundation is observed and discussed in detail. The non-dimensional pile spacing has significant effects on the wave propagation. The shadowing of the waves to Pile 2 caused by Pile 1 decreases as the non-dimensional pile spacing increases, which leads to a lower wave velocity when the wave crest reaches to Pile 2. When the non-dimensional pile spacing $l_p/D \geq 4$, the shadowing effect almost disappears.
- (2) The characteristics of Pile 1 and Pile 2 under wave loading are compared in three typical time instances and the results show that there exists some differences which are due to the phase difference between the two piles and the shadowing effect. The maximum positive and negative bending moment appears at the position $z = -1.5$ m and near the pile head, separately. Both the pore pressure and displacement of pile have their maximum values at the pile head and decrease along the vertical direction. It is worth notice that either the maximum values of pore pressure, bending moment or displacement of Pile 2 are lower than Pile 1 due to the shadowing effect by Pile 1.
- (3) The platform combines the 2×2 array of piles together as a rigid structure compared to the pile foundation without platform. The existence of the platform has significant effects on the seabed and structure dynamic response under wave loading. For both the bending moment and displacement of piles, the maximum values decrease significantly and the distributions along the piles are changed. The existence of the platform has little effects to the pore pressure due to it is mainly influenced by the seabed and wave characteristics.
- (4) The influences of wave, pile and seabed parameters on the wave-induced seabed and pile foundation platform are significant. The pore pressure is closely relative to the above parameters except the pile insertion ratio. The wave and pile parameters affect the bending moment and displacement of pile significantly, however, the seabed parameters are little effects.

Acknowledgments

The study is supported by National Natural Science Foundation of China with Grant (Project nos. 41372286, 41572243 and 41330633).

References

- Au, M.C., Brebbia, C.A., 1983. Diffraction of water waves for vertical cylinders using boundary elements. *Appl. Math. Model.* 7, 106–114.
- Biot, M.A., 1962. Mechanics of deformation and acoustic propagation in porous media. *J. Appl. Phys.* 33, 1482–1498.
- Biot, M.A., 1956. Theory of propagation of elastic waves in a fluid-saturated porous solid. I. Low-frequency range. *J. Acoust. Soc. Am.* 28, 168–178.
- Bushnell, M.J., 1977. Forces on Cylinder Arrays in Oscillating Flow.
- Chakarabarti, S.K., Tam, A., 1975. Interaction of waves with large vertical cylinder. *J. Sh. Res.* 19, 23–33.
- Chen, C.Y., Hsu, J.R.C., 2005. Interaction between internal waves and a permeable seabed. *Ocean Eng.* 32, 587–621. <http://dx.doi.org/10.1016/j.oceaneng.2004.08.010>.
- Cu ellar, P., Bae ler, M., R ucker, W., 2012. Pore-pressure accumulation and soil softening around pile foundations for offshore wind turbines. In: ASME 2012 International Conference on Ocean, Offshore and Arctic Engineering, pp. 219–228.
- Eicher, J.A., Guan, H., Jeng, D.S., 2003. Stress and deformation of offshore piles under structural and wave loading. *Ocean Eng.* 30, 369–385.
- Gade, H.G., 1958. Effects of a nonrigid, impermeable bottom on plane surface waves in shallow water. *J. Mar. Res.* 16, 61–82.
- Hirt, C.W., Nichols, B.D., 1981. Volume of fluid (VOF) method for the dynamics of free boundaries. *J. Comput. Phys.* 39, 201–225.
- Hirt, C.W., Sicilian, J.M., 1985. A porosity technique for the definition of obstacles in rectangular cell meshes. In: International Conference on Numerical Ship Hydrodynamics, 4th. Washington, D.C., pp. 1–19.
- Hsiao, S.V., Shemdin, O.H., 1980. Interaction of ocean waves with a soft bottom. *J. Phys. Oceanogr.* 10.
- Hsu, J.R.C., Jeng, D.S., 1994. Wave-induced soil response in an unsaturated anisotropic seabed of finite thickness. *Int. J. Numer. Anal. Methods Geomech.* 18, 785–807.
- Hsu, T.J., Sakakiyama, T., Liu, L.F., 2002. A numerical model for wave motions and turbulence flows in front of a composite breakwater. *Coast. Eng.* 46, 25–50.
- Jeng, D.S., 2001. A new wave dispersion equation: effects of soil characteristics. *J. Offshore Mech. Arct. Eng.* 123, 177. <http://dx.doi.org/10.1115/1.1408612>.
- Jeng, D.S., Cha, D.H., 2003. Effects of dynamic soil behavior and wave non-linearity on the wave-induced pore pressure and effective stresses in porous seabed. *Ocean Eng.* 30, 2065–2089.
- Jeng, D.S., Rahman, M.S., Lee, T.L., 1999. Effects of inertia forces on wave-induced seabed response. *Int. J. Offshore Polar Eng.* 9, 307–313.
- Jeng, D.S., Seymour, B.R., 1997. Response in seabed of finite depth with variable permeability. *J. Geotech. Geoenviron. Eng.* 123, 902–911.
- Jeng, D.S., Ye, J.H., Zhang, J.S., Liu, P.L.F., 2013. An integrated model for the wave-induced seabed response around marine structures: model verifications and applications. *Coast. Eng.* 72, 1–19. <http://dx.doi.org/10.1016/j.coastaleng.2012.08.006>.
- Karunarathna, S.A.S.A., Lin, P., 2006. Numerical simulation of wave damping over porous seabeds. *Coast. Eng.* 53, 845–855. <http://dx.doi.org/10.1016/j.coastaleng.2006.05.003>.
- Kothe, D.B., Rider, W.J., 1998. Reconstructing volume tracking. *J. Comput. Phys.* 141, 112–152.
- Lauder, B.E., Spalding, D.B., 1974. The numerical computation of turbulent flows. *Comput. Methods Appl. Mech. Eng.* 3, 269–289.
- Li, X.-J., Gao, F.-P., Yang, B., Zang, J., 2011. Wave-induced pore pressure responses and soil liquefaction around pile foundation. *Int. J. Offshore Polar Eng.* 21, 233–239.
- Lin, Y.S., Jeng, D.S., 1997. The effects of variable permeability on the wave-induced seabed response. *Ocean Eng.* 24, 623–643.
- Liu, P.L.F., 1973. Damping of water waves over porous bed. *J. Hydraul. Div.* 99, 2263–2271.
- Liu, P.L.-F., Park, Y.S., Lara, J.L., 2007. Long-wave-induced flows in an unsaturated permeable seabed. *J. Fluid Mech.* 586, 323–345. <http://dx.doi.org/10.1017/S0022112007007057>.
- Lu, J.-F., Jeng, D.-S., 2008. Dynamic response of a porous seabed and an offshore pile to linear water waves. In: ASME 2008 International Conference on Offshore Mechanics and Arctic Engineering, pp. 615–622.
- Madsen, O.S., 1978. Wave-induced pore pressures and effective stresses in a porous bed. *Geotechnique* 28, 377–393.
- Masuoka, T., Takatsu, Y., 1996. Turbulence model for flow through porous media. *Int. J. Heat Mass Transf.* 39, 2803–2809.
- Mei, C.C., Foda, M.A., 1981. Wave-induced responses in a fluid-filled poro-elastic solid with a free surface—a boundary layer theory. *Geophys. J. R. Astron. Soc.* 66, 597–631.
- Mei, C.C., Liu, K., 1987. A bingham-plastic model for a muddy seabed under long waves. *J. Geophys. Res. Atmos.* 92, 14581–14594.
- Mitwally, H., Novak, M., 1987. Response of offshore towers with pile interaction. *J. Eng. Mech.* 113, 1065–1084.
- Moshagen, H., Torum, A., 1975. Wave induced pressures in permeable seabeds. *J. Waterw. Harb. Coast. Eng. Div.* 101, 49–57.
- Mostafa, A., Mizutani, N., Iwata, K., 1999. Nonlinear wave, composite breakwater, and seabed dynamic interaction. *J. Waterw. Port Coast. Ocean Eng.* 125, 88–97. [http://dx.doi.org/10.1061/\(ASCE\)0733-950X\(1999\)125:2\(88\)](http://dx.doi.org/10.1061/(ASCE)0733-950X(1999)125:2(88)).
- Nakayama, A., Kuwahara, F., 1999. A macroscopic turbulence model for flow in a porous medium. *J. Fluids Eng.* 121, 427–433.
- Orlanski, I., 1976. A simple boundary condition for unbounded hyperbolic flows. *J. Comput. Phys.* 21, 251–269. [http://dx.doi.org/10.1016/0021-9991\(76\)90023-1](http://dx.doi.org/10.1016/0021-9991(76)90023-1).
- Raman, H., Jothishankar, N., Venkatanarasiah, P., 1977. Nonlinear wave interaction with vertical cylinder of large diameter. *J. Sh. Res.*
- Rodi, W., 1993. *Turbulence Models and Their Application in Hydraulics*. CRC Press.
- Seymour, B.R., Dong, S.J., Hsu, J.R.C., 1996. Transient soil response in a porous seabed with variable permeability. *Ocean Eng.* 23, 27–46.
- Sleath, J.F.A., 1970. Wave-induced pressures in beds of sand. *J. Hydraul. Div.* 96,

- 367–378.
- Sui, T., Zhang, J., Zheng, J., Zhang, C., 2013. Modeling of wave-induced seabed response and liquefaction potential around pile foundation. In: ASME 2013 International Conference on Ocean, Offshore and Arctic Engineering. pp. 161–170.
- Sanz-Serna, J.M., Spijker, M.N., 1986. Regions of stability, equivalence theorems and the Courant-Friedrichs-Lewy condition. *Numer. Math.* 49, 319–329.
- Ulker, M.B.C., Rahman, M.S., Jeng, D.S., 2009. Wave-induced response of seabed: various formulations and their applicability. *Appl. Ocean Res.* 31, 12–24.
- Yamamoto, T., 1981. Wave-induced pore pressures and effective stresses in inhomogeneous seabed foundations. *Ocean Eng.* 8, 1–16.
- Yamamoto, T., 1977. Wave-induced instability in seabeds. In: ASCE Special Conference, Coastal Sediments 77. Charleston, SC, pp. 898–913.
- Yamamoto, T., Koning, H.L., Sellmeijer, H., Hijum, E. van, 1978. On the response of a poro-elastic bed to water waves. *J. Fluid Mech.* 87, 193–206.
- Ye, J., Jeng, D., Wang, R., Zhu, C., 2013. Validation of a 2-D semi-coupled numerical model for fluid-structure-seabed interaction. *J. Fluids Struct.* 42, 333–357. <http://dx.doi.org/10.1016/j.jfluidstructs.2013.04.008>.
- Ye, J., Jeng, D.S., Chan, A.H.C., Wang, R., Zhu, Q.C., 2016. 3D Integrated numerical model for fluid-structures-seabed interaction (FSSI): elastic dense seabed foundation. *Ocean Eng.* 115, 107–122. <http://dx.doi.org/10.1016/j.oceaneng.2016.01.003>.
- Yuhi, M., Ishida, H., 1998. Analytical solution for wave-induced seabed response in a soil-water two-phase mixture. *Coast. Eng. J.* 40, 367–381. <http://dx.doi.org/10.1142/S0578563498000212>.
- Zhang, H., Sun, X., Wang, Y., Yin, J., Wang, C., 2015. Dynamic characteristics and simplified numerical methods of an all-vertical-piled wharf in offshore deep water. *China Ocean Eng.* 29, 705–718.
- Zhang, Y.L., Li, J., 2011. Effect of seabed motion on offshore wind turbine monopile. *Port Waterw. Eng.*
- Zhou, X.-L., Xu, B., Wang, J.-H., Li, Y.-L., 2011. An analytical solution for wave-induced seabed response in a multi-layered poro-elastic seabed. *Ocean Eng.* 38, 119–129. <http://dx.doi.org/10.1016/j.oceaneng.2010.10.003>.
- Zhou, X.-L., Zhang, J., Wang, J.-H., Xu, Y.-F., Jeng, D.-S., 2014. Stability and liquefaction analysis of porous seabed subjected to cnoidal wave. *Appl. Ocean Res.* 48, 250–265. <http://dx.doi.org/10.1016/j.apor.2014.09.005>.
- Zienkiewicz, O.C., Chang, C.T., Bettess, P., 1980. Drained, undrained, consolidating and dynamic behaviour assumptions in soils. *Geotechnique* 30, 385–395.